Los Alamos National Laboratory is operated by the University of California for the United States Department of Energy under contract W-7405-ENG-36

LA-UR--87-2853

DE87 014757

TITLE CONCEPTUAL DESIGN OF A HIGH-RESOLUTION π^0 SPECTROMETER

AUTHOR(S): J. David Bowman
Los Alamos National Laboratory

SUBMITTED TO The Proceedings of the Workshop on Photon and Neutral Meson Physics at Intermediate Energies, Los Alamos National Laboratory, Los Alamos, NM January 7-9, 1987

DISCLAIMER

Los Alamos Los Alamos National Laboratory
Los Alamos, New Mexico 87545

FORM NO. 836 R4
ST. NO. 2629 5/81

CONCEPTUAL DESIGN OF A HIGH-RESOLUTION π^0 SPECTROMETER

J. David Bowman
Los Alamos National Laboratory

I will discuss the design of a high-resolution π^0 spectrometer based on accurate measurements of the opening angle between the two γ rays from π^0 decay. The first π^0 spectrometer of this type was built at LAMPF and first operated in 1978. It has an energy resolution of 2 MeV and solid angle of about 1 msr. The design and performance of the LAMPF π^0 spectrometer, as well as the physical principles of the opening angle π^0 spectrometer, are discussed in Ref. 1.

During the last 10 years a considerable body of work studying the π-nucleus and π-nucleon charge-exchange reaction has been carried out. Many experiments that are being proposed and considered require a more capable instrument.

During the same period there has been substantial improvement in the technologies of photon calorimetry and charged particle vertex resolution. These improvements make possible a ten-fold improvement in the energy resolution of a π^0 spectrometer. It is also possible to achieve large improvements in solid-angle and rate capabilities. I will review and develop the physical principles involved in the design of an opening angle π^0 spectrometer. I will show that these principles, combined with the goals of good energy resolution, large-solid angle, and high-rate capability, constrain the design of a practical instrument.

To establish the basis for discussion of solid-angle, energy resolution, and rate, it is necessary to consider beams, targets, cross sections, and experiments. To be specific, the LEP channel at LAMPF[2] provides charged pion beams with $\Delta p/p$ as small as 10^{-3} and fluxes as large as $10^9 \pi^+$s/sec. Cross sections for nuclear π charge-exchange reactions on nuclear targets range downward from 1 mb/sr. For a real experiment, the beam and target as well as the detector contribute to the energy resolution. Consider the situation where the beam target and spectrometer all give the same contribution to the energy resolution. For a momentum bite $\Delta p/p = 10^{-3}$ at $T_\pi = 150$, the beam energy resolution is 0.22 MeV (FWHM), and the flux is $1.5 \cdot 10^7 \pi^+$/sec. A ^{13}C target of 0.6 gm cm^{-2} contributes 0.22 MeV of ionization energy-loss straggling.[3] I will show below that a spectrometer contribution of 0.22 MeV is feasible. The overall energy resolution is then

$$0.22 \cdot \sqrt{3} = 0.38 \text{ MeV} .$$

For a 0.22-MeV energy resolution a 2 msr solid angle is attainable. The yield is then 75 counts/day for a 1 μb/sr cross section. The above spectrometer characteristics would make possible an extensive program of study of pion charge-exchange reactions leading to discrete final states. Isobaric-analog states could be studied to momentum transfers corresponding to the third diffraction maximum. Weaker states could be studied out to the second diffraction maximum. This would allow the experimental characterization of the π-nucleus isovector optical potential and the quantitative use of the π charge-exchange reaction for the study nuclear structure. The large solid angle would allow experiments to be performed in a few days time.

There are several design goals for a π^0 spectrometer, some of which conflict. These include:

(1) Minimum cost,

(2) Good energy resolution,

(3) Large solid angle,

(4) High rate capability, and

(5) Highly selective trigger.

In addition it is necessary that the ratio of data-taking time to calibration and servicing time be large. I will discuss how these design goals and available detector technology constrain the design of a π^0 spectrometer. Conversely, I will show that a spectrometer is feasible which achieves a system resolution of 0.4 MeV at a solid angle of 2 msr. A solid angle as large as 5 msr and a spectrometer resolution as small as 0.05 MeV are possible. The cost is of the order of $\$2.5 \times 10^6$ and cannot be drastically reduced.

The spectrometer design I will discuss is based on measuring the direction and energies of the two γ's from the decay $\pi^0 \rightarrow \gamma\gamma$. Figure 1 shows some relationships in the kinematics of π^0 decay. There are two independent ways of determining the π^0 energy from laboratory quantities.

$$\omega_1 = E_1 + E_2 \tag{1}$$

$$\omega_2 = m\sqrt{(1 - \cos\eta)(1 - x^2)} \tag{2}$$

where

$$x = \frac{E_1 - E_2}{E_1 + E_2}\beta\cos\theta^* \ . \tag{3}$$

The laboratory opening angle η is a minimum for events where the two γ energies are the same. For these events $x = 0$, $\theta^* = \pi/2$, and the phase space $(\sin\theta^* d\theta^* d\phi^*)$ is a

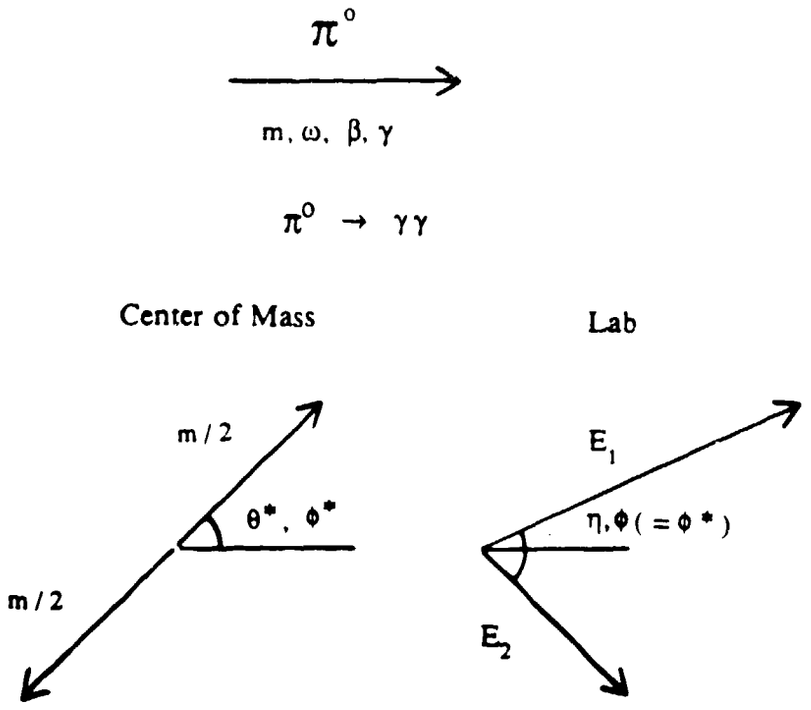

Fig. 1. The symbols have their conventional definitions: m, ω, β, and γ are the mass, total energy, velocity, and energy-to-mass ratio of the π^0 in the laboratory frame. In the π^0 rest frame the Z axis is taken along the laboratory momentum. The decay γ's lie along or against the directions specified by the polar angle θ^* and azimuthal angle ϕ^*. The γ's each have energy $m/2$. In the laboratory frame the two γ's have energies E_1 and E_2, opening angle η, and azimuthal angles $\phi_1 = \phi_1^*$, $\phi_2 = \phi_2^*$.

maximum. Equation (2) gives a much more accurate determination of ω than Eq. (1). The comparison of ω_1 and ω_2 on an event-by-event basis can serve to eliminate background. The π^0 direction can be accurately determined from the direction of the momentum sum of the two γ's.

Figure 2 shows conceptually how the energies and directions of the two γ's are measured. Each of the γ's is converted into an e^+e^- pair in a pair of active converters. The e^+e^- vertex is reconstructed by a tracking chamber behind the converter (there may be

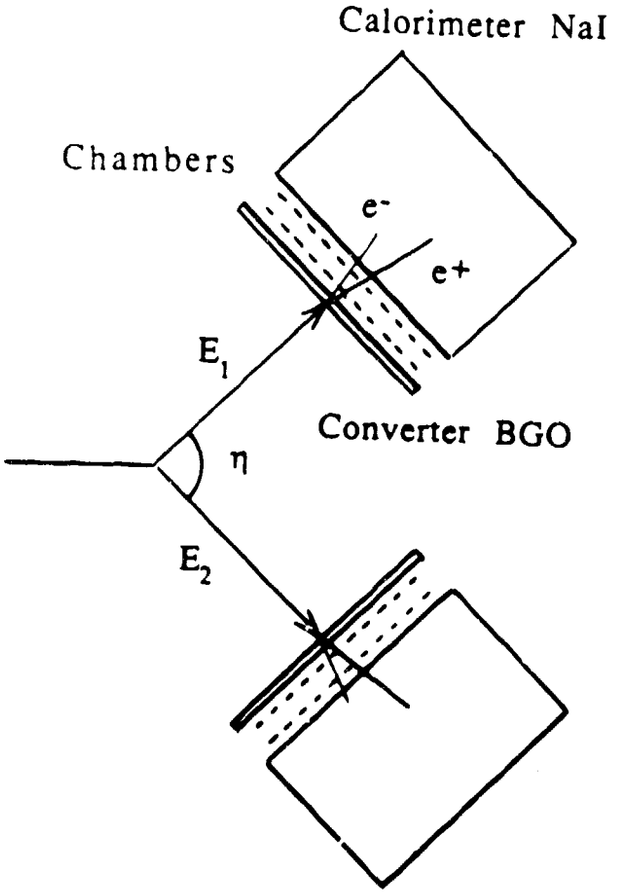

Fig. 2. Shows how η, E_1, and E_2 are measured.

more than one converter per arm). The e^+e^- pair develops an electromagnetic shower. The total shower energy is determined by adding the signal from calorimetric detectors, which absorb the shower energy, to the energy deposited in the active converters.

The first round of questions that arises is:

(1) How does the γ-ray energy resolution enter into the π^0 energy resolution?

(2) What is the most cost effective material for the calorimeter?

(3) How does the opening-angle resolution enter into the π^0 energy resolution?

(4) What is the most cost effective material for the converter?

The measured γ energies enter the expression for the π^0 energy as follows.[1] Expanding $\omega\ (\omega \quad \omega_2)$ as a function of x about $x \quad x_0$ yields

$$\omega(x) \quad \omega + \frac{\partial\omega}{\partial x}(x \quad x_0) + \frac{1}{2}\frac{\partial^2\omega}{\partial x^2}(x \quad x_0)^2 \qquad (4a)$$

$$\omega(x) = \omega\left(1 + x_0(x - x_0) + \frac{1}{2}(x - x_0)^2\right) + \ldots \tag{4b}$$

for $x_0 = 0$. The term linear in $x - x_0$ vanishes. This is the reason it is possible to obtain good π^0 energy resolution in the first place. For symmetric decays ($x = 0$) the π^0 energy only depends on the opening angle η and not on x. In order to obtain the spread in ω, $\Delta\omega$, it is necessary to keep the term quadratic in $(x - x_0)$. If ΔE_γ is the fractional γ-ray energy resolution at $E_\gamma = \omega/2$, then for $x = 0$ the π_0 energy resolution is

$$\Delta\omega_{\rm RMS} = \frac{1}{2\sqrt{2}}\omega(\Delta E_\gamma)^2$$

for NaI at 140 MeV ($T_{\pi_0} = 140$ MeV). $\Delta E_\gamma \sim 1.7\%$, so

$$\Delta\omega_{\rm RMS} = 30 \text{ keV} \quad .$$

This extremely small value of the π^0 energy resolution only holds when an extremely narrow range of x near $x = 0$ is accepted. In fact, the distribution of reconstructed π^0 energies ω is highly non-Gaussian in this situation and the full-width, half-max resolution is about the same as the root-mean-squared resolution. The opening-angle resolution contribution can be made arbitrarily small by making the target-to-detector distance R large. Using a NaI calorimeter and very restrictive x acceptance it is possible to obtain a spectrometer resolution of 30 keV!

In a practical situation, a finite range of x, say from $-y$ to $+y$, must be accepted in order to obtain a large acceptance. In this case the linear term in (Eq. (4b)) contributes and

$$\frac{\Delta\omega}{\omega} = \frac{1}{\sqrt{12}} y \Delta E_\gamma \tag{5}$$

The γ-ray energy resolution is still extremely important. For fixed $\Delta\omega$ the value of ΔE_γ determines the range of x that can be accepted. Recall that x ranges from $-\beta$ to $+\beta$. For $y \gg \Delta E_\gamma^2$ the ω distribution is approximately Gaussian. If $\Delta\omega = 0.14$ MeV FWHM is desired, then the fractional x acceptance at $T_{\pi_0} = 100$ MeV is

$$\frac{y}{\beta} = 6.0\% \quad .$$

Now we are ready to select a calorimeter material. Table I summarizes some of the properties of commercially available candidate calorimeter materials. The depth of the calorimeter must be 16 to 20 radiation lengths deep to contain a 1-GeV electromagnetic

Table I. Properties of detector materials. The energy resolution is for modular detectors and does not represent the best that can be obtained with a monolithic detector.

Detector Material	$\Delta E/E$ *at 100 MeV*	*Cost/cm*^{3}	*Radiation Length*
Pb Glass	30%	\$0.5	2-4 cm
NaI	4%	\$2	2.5 cm
BGO	4%	\$20	1.1 cm

shower so the relevant cost figure is cost (cm^2 $\times$ radiation length). From the point of view of energy resolution, both NaI and BGO are much better than lead glass. Figure 3 compares the energy resolution of NaI and BGO detectors. From the point of view of cost, NaI is much better than BGO. Therefore, NaI is the material of choice for the calorimeter. NaI and BGO have comparable energy resolution at high energies.

Now consider the influence of opening angle resolution on the π^0 energy resolution.

$$\frac{\partial \omega}{\partial \eta} = m\gamma^2 \frac{1}{2} \cos\frac{\eta}{2} \tag{6}$$

for $\gamma = 2$, $T_{\pi_0} = 140$ MeV, $\eta = 60^\circ$.

$$\frac{\partial \omega}{\partial \eta} = \sqrt{3}\ \mathrm{m}$$

for $\Delta\omega = 0.140$ keV (FWHM), $\Delta\eta = 6 \times 10^{-4}$ Rad (FWHM). Take a target to detector distance of 1 m. Then

$$\Delta\eta = \frac{\sqrt{2}\Delta V}{R}$$

where ΔV is the vertex resolution, so

$$\Delta V = 0.24\ \mathrm{mm\ RMS}$$

is required! I will argue that it is possible to obtain this vertex resolution.

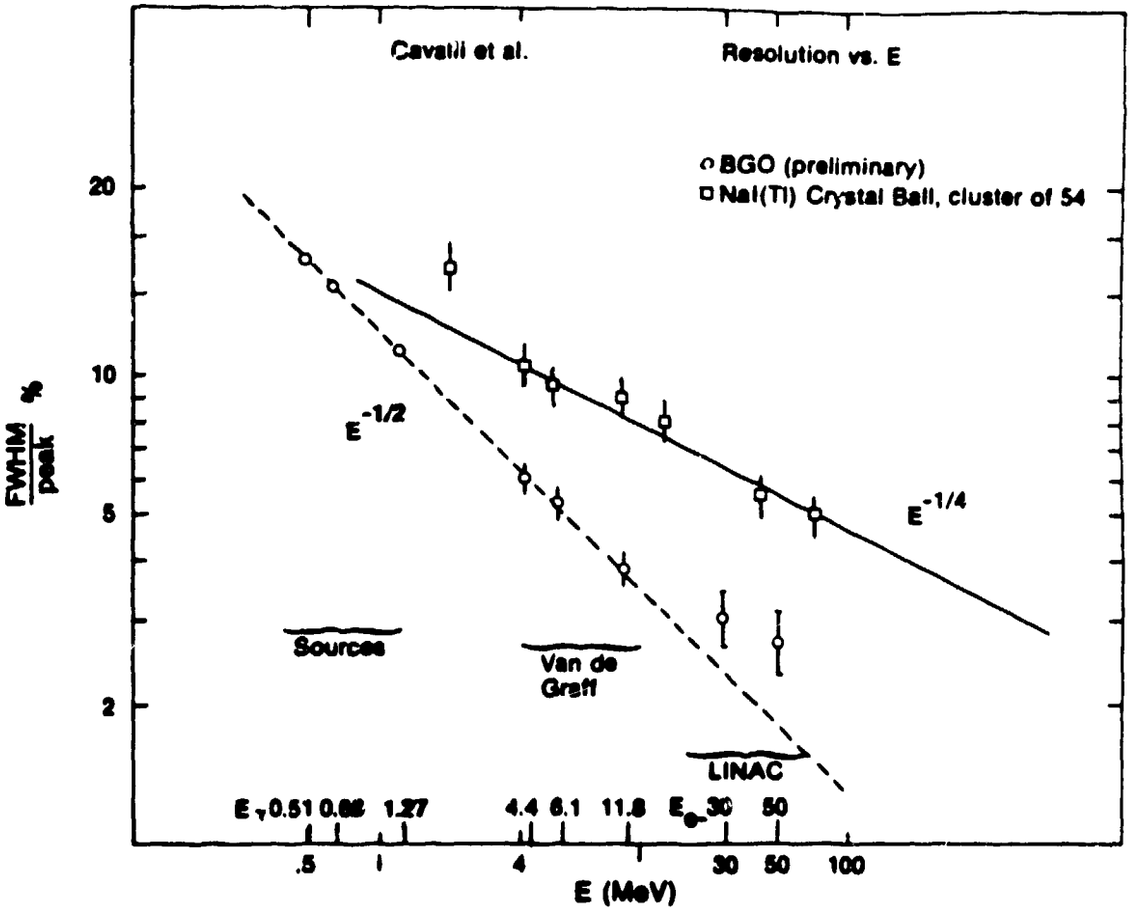

Fig. 3. Compares the energy resolution of NaI and BGO.

When a γ ray having an energy greater than a few MeV interacts with matter, it produces an electromagnetic shower through successive pair production and bremsstrahlung processes.[4] The characteristic length for a γ ray to produce a pair or for an electron to emit a hard γ is called the radiation length X_0. This same characteristic length governs the multiple scattering of charged particles, which is expressed by the relation[5]

$$\sigma_\theta = \frac{15\ \text{MeV}}{pv}\sqrt{\frac{X}{X_0}}\ . \qquad (7)$$

Here σ_θ is the RMS scattering angle projected on one coordinate, X is the thickness of material through which the charged particle passes, v is the particle velocity and p is the particle momentum. The same characteristic length X_0 applies to the three processes pair production, bremsstrahlung, and multiple scattering—because they all result from

the interaction of the projectile with the screened Coulomb field of the target or medium nuclei.

The requirements of high conversion efficiency and good vertex resolution are contradictory. For $X \ll X_0$ the conversion probability P_c is proportional to X/X_0

$$P_c \sim X/X_0 \quad . \tag{8}$$

The vertex resolution ΔV is proportional to X times the RMS scattering angle σ_θ

$$\Delta V \sim X \frac{15}{pv} \sqrt{\frac{X}{X_0}} \sim X_0 \frac{15}{pv} \left(\frac{X}{X_0} \right)^{3/2} \quad . \tag{9}$$

For ΔV small, we want X/X_0 small; for P_c large, we want X/X_0 large. For fixed conversion probability, the vertex resolution is minimized by choosing a material with a small X_0. The material of choice is BGO, which has a 2.3 times smaller radiation length than NaI. Since the γ-ray energy resolution of BGO is comparable to that of NaI and only a small fraction of the energy is deposited in the BGO, the overall γ-ray energy resolution can be expected to be 4% at 100 MeV.

I showed above that a vertex resolution of 0.24 mm RMS was required. How can such a small vertex resolution be obtained? E. B. Hughes and Y. C. Liu[6] of Stanford University have made a Monte Carlo study of this problem using the computer code EGS.[7] Dan Sober of Catholic University has also tackled this problem and his results, which are similar to those of Hughes and Liu, are reported in these proceedings. I will report the results of the Hughes and Liu work.

Consider a slab of BGO having thickness X. As X is increased, the shower develops more before the shower products emerge from the back of the slab. Figure 4 shows the number of charged-particle tracks emerging from the back of a converter slab as a function of the slab thickness for a 150-MeV incident γ ray. For small thicknesses ($\sim$0.5 X_0), two-prong events dominate as expected. At large thicknesses ($\sim$2.0 X_0), the probability of one or more charged prongs to emerge begins to saturate as the shower becomes highly developed.

What is the best algorithm with which to reconstruct the interaction vertex? First consider a one-prong event. Let y and θ_y be the y coordinate and y projected angle of the particle as it emerges from the connector. These, as well as other quantities, are shown in Figure 5. The most general vertex estimator, which is linear in θ, can be written as

$$y' = y + l\theta_y \quad . \tag{10}$$

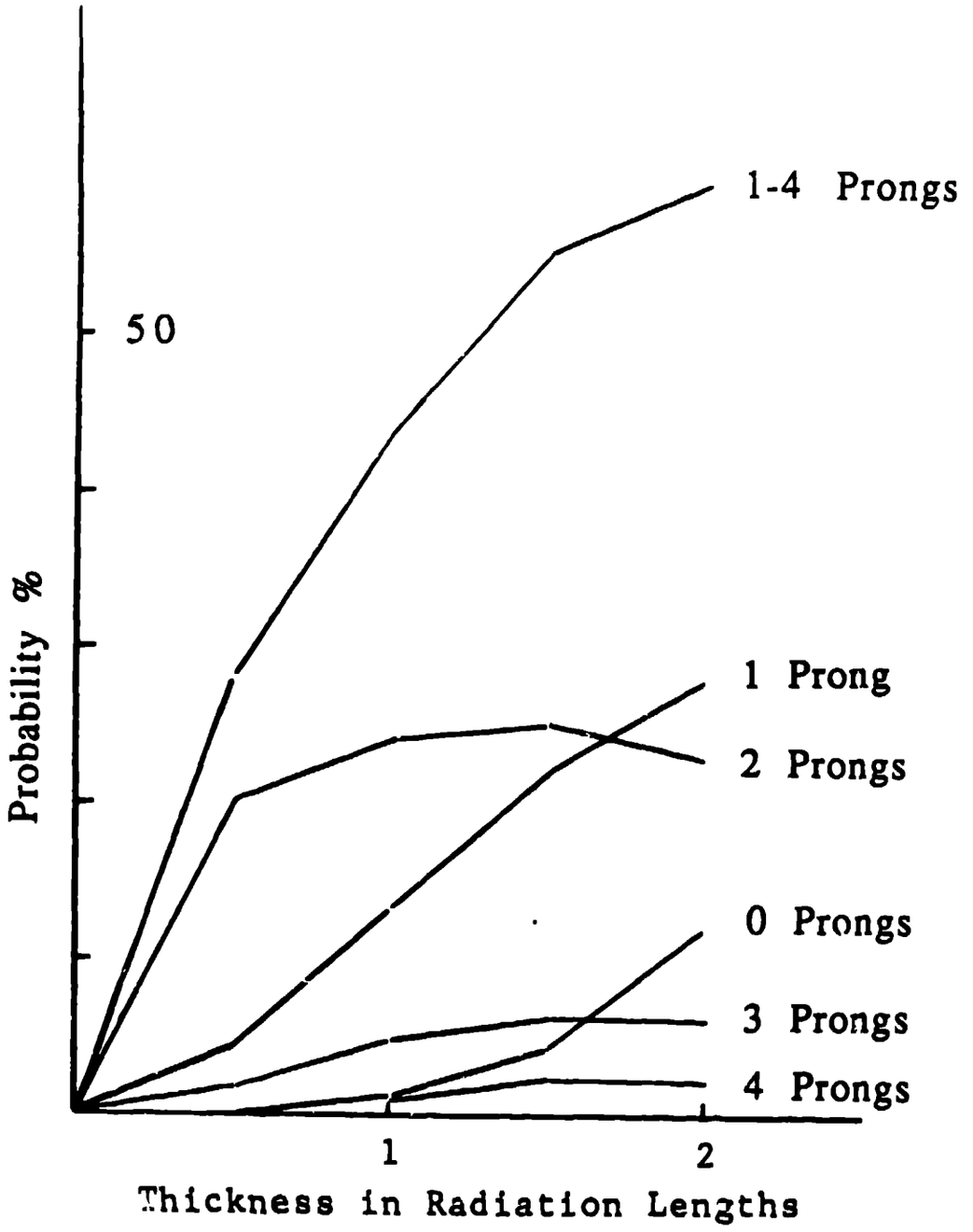

Fig. 4. Shows the probability of different numbers of prongs emerging from the back of a BGO slab as a function of the slab thickness. The zero-prong events are from photons that interact in the slab but for which no charged particles emerge.

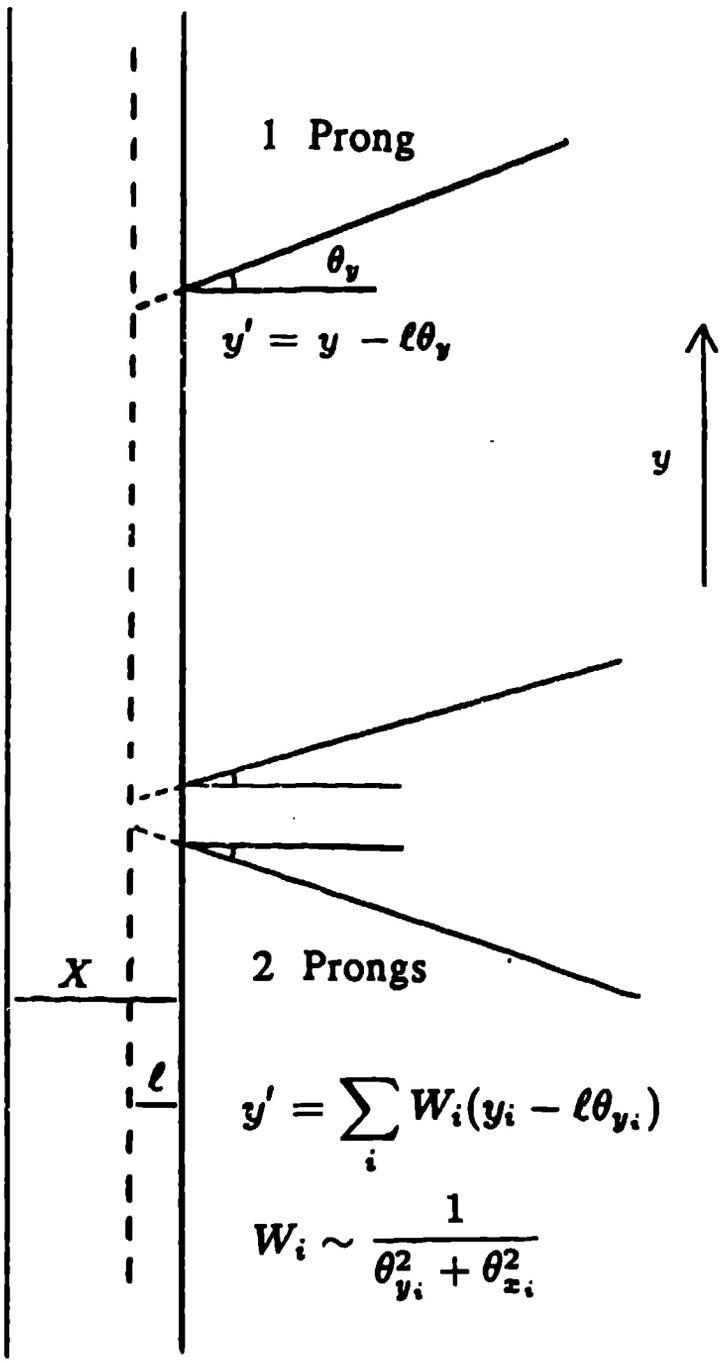

Fig. 5. Illustrates the vertex reconstruction algorithm for one- and two-prong events.

The y coordinate of the origin of the track is obtained by projecting the track to a depth ℓ in the slab. The RMS deviation of this estimator from the true vertex y coordinate is shown in Fig. 6 as a function of ℓ/X. If more than one prong is present, then a reasonable algorithm is obtained by forming a weighted average of the individual estimate for each prong

$$y' = \sum_i W_i(y_i - \ell\theta_{y_i}) \tag{11}$$

with

$$W_i \sim \frac{1}{\theta_{y_i}^2 + \theta_{x_i}^2}$$

The weighting factor is proportional to the inverse of the space angle squared. This weighting emphasizes the forward-going prongs that are likely to have high energies and to have suffered less multiple scattering than those prongs observed to have large angles. The vertex resolution is plotted versus ℓ/X for one-, two-, and three-prong events for 0.5, and 1.0 thick converters. In Fig. 6 the optimum ℓ/X has been determined for each class of event (number of prongs) and the optimized vertex resolution is plotted versus $X^{3/2}$ in Fig. 7. The vertex resolution is seen to increase somewhat faster than the $X^{3/2}$ predicted by Eq. (9) as a result of the increase in shower complexity as X increases. A vertex resolution of 0.24 mm can be obtained for a converter thickness of 0.5 X_0. The rapid increase of the vertex resolution with X makes the use of a thicker converter impossible. According to Fig. 4 the conversion probability is 28% for a 0.5 X_0 thick converter.

Next consider the problem of choosing a tracking detector. Two types of tracking chambers are available: drift chambers and multiwire proportional chambers. The latter are excluded by their inherently poor positive resolution, 0.6 mm RMS for 2-mm wire spacing. Drift chambers employing drift distances of 1 cm obtain a position resolution of 0.1 mm RMS. The cost of commercial readout is approximately \$200/wire. The Lecroy "pipe line TDC" provides a pulse pair resolution of ~2 mm, so that hits separated by more than this separation can be resolved. For converters 0.5 radiation lengths or thicker, the drift-chamber resolution of 0.1 mm is small compared to the theoretical vertex resolution from the algorithm and will not significantly degrade the theoretical vertex resolution.

The designing and configuration of the drift chambers must balance the following requirements:

(1) One-, two-, and three-prong events must be processed.

(2) The drift chamber package must be thin along the γ propagation direction since the solid angle depends on the distance to the back of the calorimeter to the third power (see below).

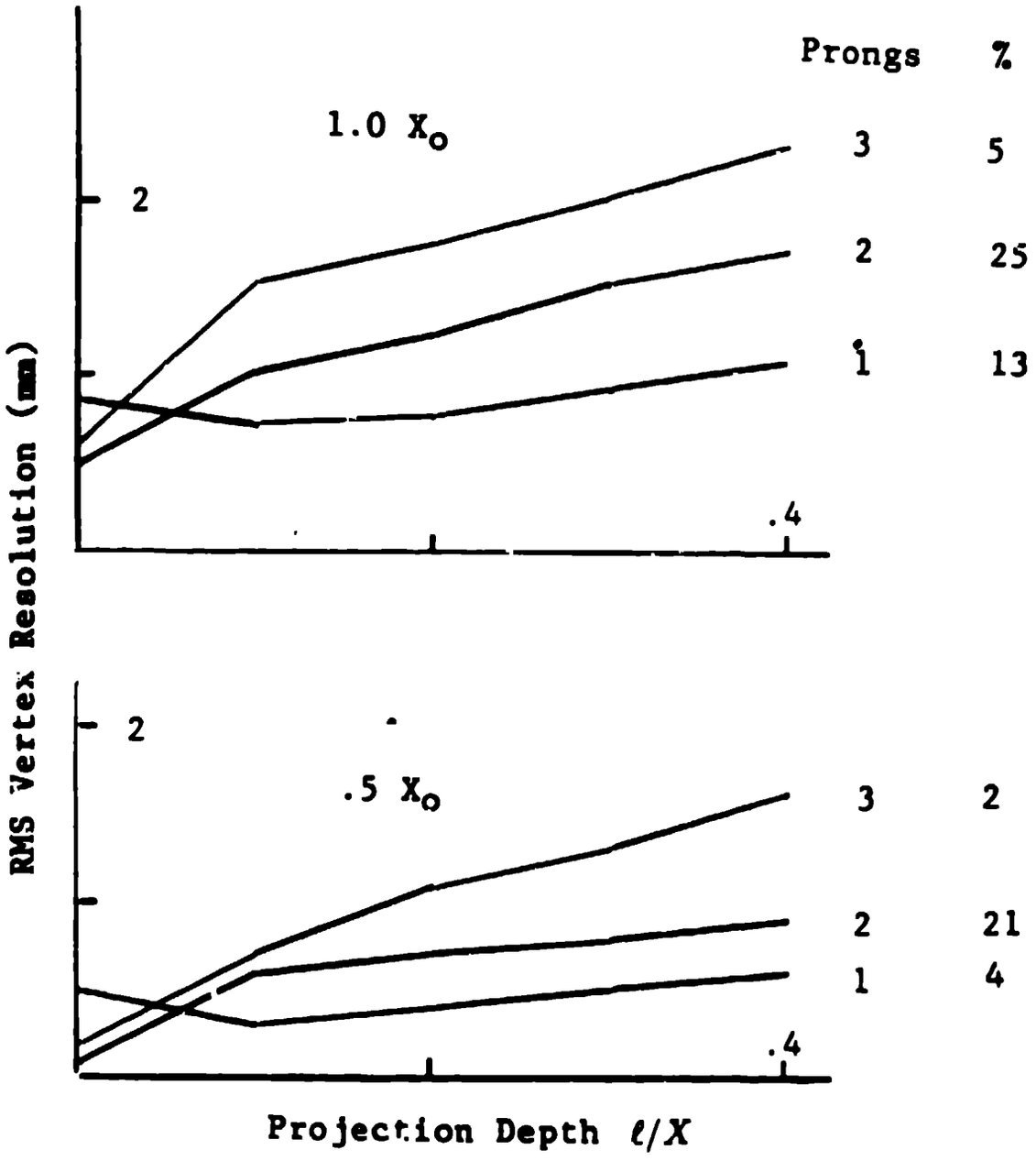

Fig. 6. Shows the RMS vertex resolution for 1-, 2-, and 3-prong events as a function of projection depth ℓ/X. Slab thicknesses of 0.5 and 1.0 radiation lengths are shown. The probabilities of each class of events are shown under %.

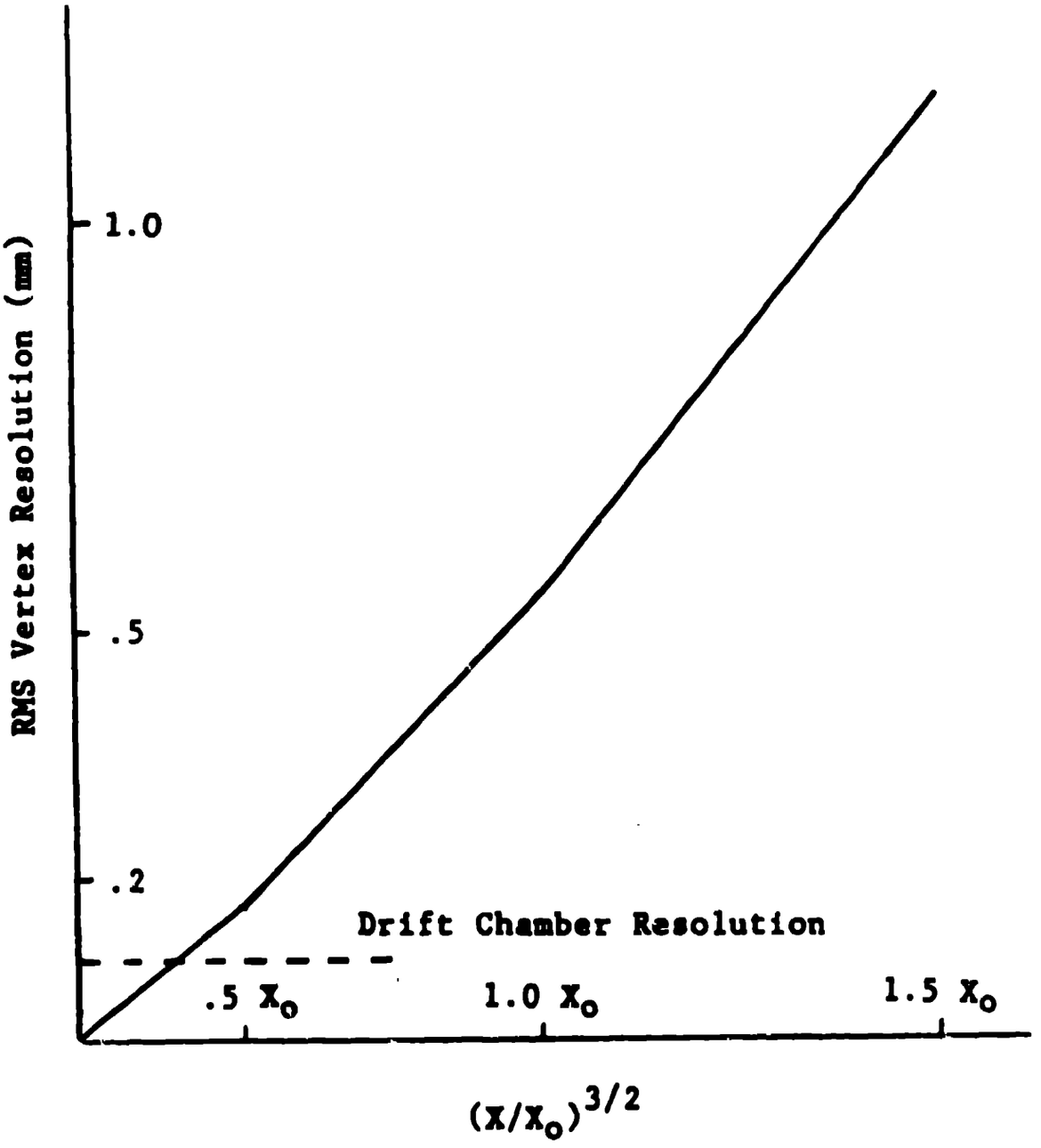

Fig. 7. Shows the optimized vertex resolution as a function of the slab thickness in radiation lengths to the 3/2 power. The 0.1-mm drift chamber resolution is shown for reference.

(3) For fast on- and off-line analysis, a simple geometry is desirable.

(4) The reconstruction algorithm should handle missing and overlapping hits.

I have studied a detector configuration, shown in Fig. 8, that may satisfy the above criteria. The configuration consists of three sets of three planes. Each plane is 1 cm thick for a total thickness of 11 cm/converter, 9 cm chamber + 1 cm converter + 1 cm scintillator. The planes are at angles of 120° with respect to one another and arranged in an $r, s, t, r, s, t, r, s, t$ pattern. A typical two-prong event with an opening angle of 4° is shown on the figure. The tracks are separated by 7 mm at the ninth plane. There are four degrees of freedom for each track. The five-fold overdetermination of each track allows the elimination of left-right ambiguities for 99% of the tracks if the third plane in each set is displaced by 1/2 of the field to sense wire spacing.

This configuration allows a hierarchal approach to the track finding problem. The three planes in each of the r, s, and t sets are analyzed separately to give a slope and an origin. The three sets of slopes and origins are tested for compatibility, combined to give two slopes and two origins in an orthogonal coordinate system. A straightforward but tedious calculation shows that the error in the projected vertex is nearly the same as the resolution of each plane.

If there is one missing hit (9% probability for 99% efficient chambers), then the two sets that have three hits still give sufficient information to reconstruct the track with two-fold overdetermination. The hits in the incomplete plane provide two more consistency checks. As shown in Fig. 7, the typical two-prong event has a separation of 7 mm at the ninth plane and a smaller separation in the forward planes. This problem is not fatal. Suppose the two tracks were not separated at all but appeared as one track. The reconstructed origin would coincide with the origin constructed from the two tracks separately using the algorithm of Eq. (11). It should be possible to develop a good algorithm which combines unresolved hit information in the forward chambers and resolved or unresolved hit information in the back chambers to accurately reconstruct the projected track origin.

The conclusion after considering the problems of vertex detection and reconstruction are:

(1) The optimum converter material is BGO.

(2) The optimum converter thickness is about 0.5 radiation lengths, which gives 0.24 mm resolution with 28% detection efficiency.

(3) Drift chambers can provide the needed accuracy and redundancy to reconstruct one-, two-, and three-prong events.

Now we consider the problems of the efficiency of π^0 detection. Among the factors considered are:

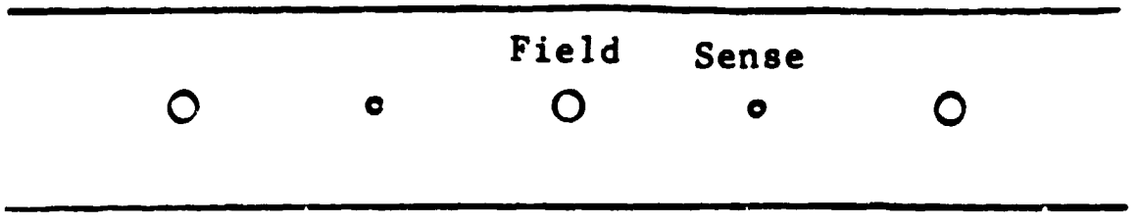

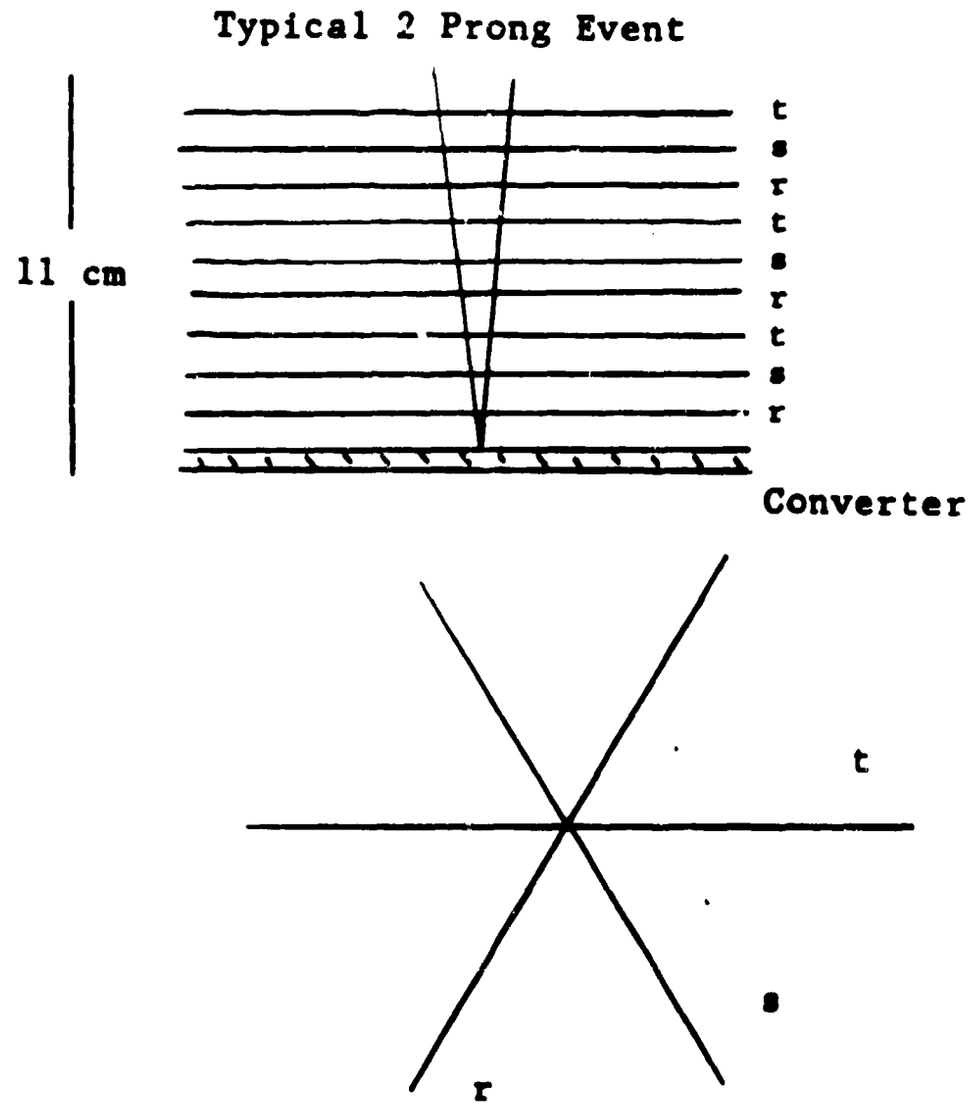

Fig. 8. Shows a possible drift-chamber configuration. The opening angle for a typical 2-prong event from a 150 MeV γ is shown.

(1) Calorimeter size and shape.

(2) Number of converters.

The solid angle Ω for π^0 detection may be defined as the detector efficiency averaged over the spectrometer acceptance. According to this definition, the probability of detecting an isotropically emitted π^0 is $\Omega/4\pi$. Note that the acceptance may extend over a solid angle as large as 1 sr, but the detector efficiency is small so that the product is of the order of a few $\times 10^{-3}$ sr.

Consider a pair of γ detectors deployed as shown in Fig. 2. An approximate formula for the solid angle is

$$\Omega = (P_{\rm conv})^2 \frac{L^2 H}{R^3} \frac{1}{2\pi \sin\eta/2 \cos\eta/2} \frac{y}{\beta} \quad . \tag{12}$$

Here $P_{\rm conv}$ is the probability that a γ is converted into charged particles that are detected, L is the detector size in the azimuthal direction, H is the detector size in the opening-angle direction, R is the source-to-detector distance, η is the opening angle, and y is the range of energy-sharing parameter x accepted. The factor $(P_{\rm conv})^2$ gives the probability that both γ's are detected, LH/R^2 is the solid angle of one γ detector, $\frac{L}{R}\frac{1}{2\pi \sin\eta/2\cos\eta/2}$ is an azimuthal acceptance factor, and (y/β) is the fractional acceptance of x. One immediately notes that the solid angle behaves like $\frac{1}{R^2}$ and not $\frac{1}{R^3}$. This behavior places a premium on making the distance from the source to the back of the calorimeter small.

It is desirable that all calorimeter modules have the same size for reasons of economy. The modules should be large enough that the outer modules can guard the inner fiducial modules from shower leakage. Identical modules allow selection of those having poor resolution to be used as guards. The modules should be large enough so as to completely contain a few MeV γ so that they can be individually calibrated using radioactive sources. The module size chosen should be compatible with the sizes of commercially available photomultiplier tubes. It is important to consider that a larger module size will require a smaller number of data channels. The size of the modules should be small enough that showers can be localized to a cluster of modules. In this way, pile-up problems can be reduced. Monte Carlo studies carried out by Hughes and Liu[6] indicate that an array of 30 cm $\times$ 30 cm of NaI is necessary to contain an electromagnetic shower of a few hundred MeV. A simple array that satisfies the above criteria is a 3 $\times$ 3 array of 10 cm $\times$ 10 cm square crystals fitted with 3-inch diameter photo tubes. The module with the highest pulse height is almost always the hit module and a 3 $\times$ 3 array centered on the high-pulse

height crystal contains the transverse shower development. A crude position value can be obtained as an energy-weighted average of module centers

$$x = \frac{\sum E_i x_i}{\sum E_i} .$$

The FWHM resolution of such a position estimator is somewhat less than half a module size.

The distance to the back of the calorimeter, R, would be smaller for a BGO calorimeter than for a NaI calorimeter. Thus, for a BGO calorimeter the area LH could be about 25% smaller so that the relative calorimeter costs for BGO and NaI would be \$250/\$80. The conclusion is still that NaI is more cost effective than BGO for the calorimeter.

How thick should the calorimeter be? The answer depends on how high energy π^0's we wish to detect. One-GeV π^0's produce 600 MeV γ's. Figure 9 shows the FWHM light responses due to shower leakage as a function of calorimeter thickness calculated by Hughes and Liu. A calorimeter thickness of 16 radiation lengths seems to be a reasonable compromise. This was the thickness used for the SLAC crystal ball.

Since the solid angle depends on L^2H, a rectangular array has a larger solid angle than a square array. Table II compares the π^0 solid angles and other characteristics of different arrays of 10 cm $\times$ 10 cm NaI modules. A 6 $\times$ 10 array is a reasonable choice. A smaller array would give much less solid angle per unit cost, and a larger array would become mechanically unwieldy.

The next question to decide is how many converters per arm to use. According to Eq. (12), the solid angle, Ω, will increase as the number of conversion planes, n is increased because $(P_{\rm conv})^2$ increases. On the other hand, as n increases, R also increases and Ω decreases since the back of the calorimeter moves further away from the source. Figure 10 shows the dependence of Ω and $P_{\rm conv}$ on n for a representative geometry. There is a dramatic increase in Ω as n increases from 1 to 2, but Ω increases less rapidly after that. The cost, \$100,000/plane, and complexity of the converters is large and so their number should be increased unless there is a clear advantage to be gained. The best choice for n is therefore 2.

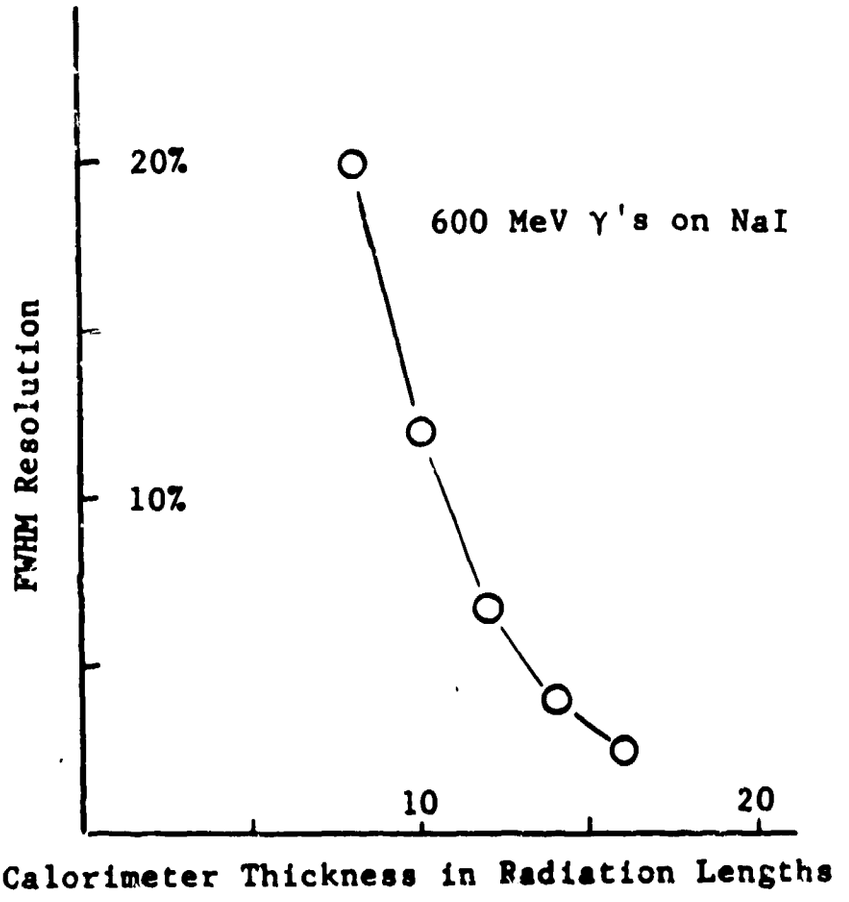

Fig. 9. Shows the contribution of shower leakage to the γ energy resolution as a function of the NaI calorimeter thickness in radiation lengths. The incident γ energy is 600 MeV.

I have modeled a spectrometer having the characteristics outlined above using the Monte Carlo code developed to describe the LAMPF π^0 spectrometer. This code is not sufficiently refined to completely describe the proposed new spectrometer, but it does include such things as finite target thickness, ionization energy loss of the incident pions, ionization energy loss straggling in the Gaussian approximation, beam momentum spread, vertex resolution, γ energy resolution, and finite detector geometry. The Monte Carlo calculation is the basis of the rate and energy resolution estimates given at the beginning

Table II. Comparison of different arrays.

Array	*Fiducial Blocks*	*k$*	*Relative* $\pi^0\Omega$	Ω/$
3 × 5	3	300	9	3.0
4 × 6	8	480	32	6.7
5 × 8	18	800	108	13.5
6 × 10	32	1200	256	21.3

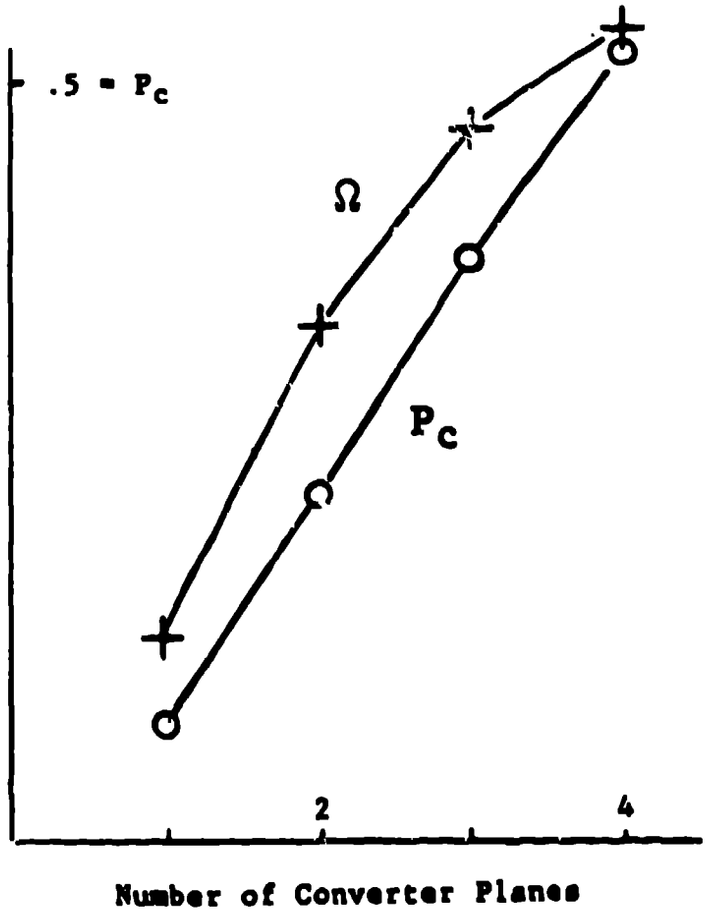

Fig. 10. Shows the probability of γ conversion and solid angle in arbitrary units as a function of the number of converter planes.

of this paper. It is possible to obtain: 0.4-MeV system energy resolution at $\Delta p/p = 10^{-3}$ and 0.6 gm/cm^2 ^{13}C target at 150 MeV pion kinetic energy. An estimated π^0 solid angle of 2 msr gives a count rate of 75 counts/day for a 1 μb/sr cross section.

Finally, in Table III the estimated costs of a new π^0 spectrometer are given. The total cost is about \$2.5 $\times$ 10^6 which is dominated by the \$1.2 $\times$ 10^6 cost of the NaI.

Table III. Estimated costs for major capital items.

Item	*Price (\$ $\times 10^6$)*
NaI 6×10^5 cm^3 at \$2/cc	1.20
BGO 10^4 cm^3 at \$20/cc	0.25
Drift Chamber Readout, 1600 Anode Wires at \$200/wire	0.32
NaI Enclosure	0.20
Support Hardware	0.15
Alignment System	0.05
Photo Tubes, Bases, 200 at \$300	0.06
Electronix	0.25
Total	2.48

I have argued that it is possible to build a π^0 spectrometer that can have a working resolution of 0.4 MeV and a solid angle of 2 msr. This instrument would be able to take data at a rate that would make possible the systematic study of isovector excitation in nuclei as well as a wide variety of reaction-mechanism and particle-physics experiments. I have argued that the current state of technology makes the instrument feasible, but there is not much room to maneuver. A serious compromise in the size or quality in any of the subsystems would yield a much inferior instrument.

REFERENCES

1. H. W. Baer, R. D. Bolton, J. D. Bowman, M. D. Cooper, F. H. Cverna, R. H. Heffner, C. M. Hoffman, N. S. P. King, Jose Piffaretti, J. Alster, A. Doron, S. Gilad, M. A. Moinester, P. R. Bevington, and E. Winkelmann, "Design, Construction, and Performance of a High-Resolution π^0 Spectrometer for Nuclear Physics Experiments," *Nuclear Instruments and Methods* **180**, 445 (1981).

2. LAMPF Users Handbook.

3. S. M. Seltzer and M. J. Beyer, "Studies in Penetration of Charged Particles in Matter," National Academy of Sciences Publication 1133.

4. An up-to-date review of electromagnetic shower and multiple scattering theory is given in Y. Tsai, *Review of Modern Physics* **46**, 815 (1974).

5. G. Z. Moliere, *Naturforsch.* **3**(a), 78 (1978).

6. E. B. Hughes and Y. C. Liu. private communication.

7. R. L. Ford and W. R. Nelson, Stanford Linear Accelerator Center Report No. SLAC-PUB-210, 1978 (unpublished).